

rapid scaling in low precision math capabilities utilized by next generation DL-networks. Moreover, the slowdown in transistor scaling along with reticle limitations in silicon lithography are restricting transistor and die area growth, making it ever harder to deliver competitive performance in multiple application domains via a single converged GPU design. Future off-chip bandwidth scaling is also at risk as the die edge scales sub-linearly with increasing die size, limiting the off-chip DRAM and I/O bandwidth available to individual dies [7].

The growing importance of DL domain specific acceleration in the datacenter is demonstrated by a proliferation of accelerators targeted exclusively at DL algorithms [22], [31], [34], [42]. We believe that the combination of technology trends and an ultra-competitive DL landscape has created an inflection point at which GPU manufacturers must embrace more domain-specialized GPU designs to continue providing competitive performance, while also maximizing design reuse and minimizing non-recurring engineering (NRE) costs.

In this work we examine historical trends and project future ratios, that show a strong divergence between high and low precision math throughput on GPUs. We show that this gap makes it difficult to design a memory system that efficiently supports both HPC and DL use cases. Thus, we propose a Composable **On-Package GPU** (COPA-GPU) architecture as a practical solution for building a new class of domain-optimized GPUs. Leveraging multi-chip module (MCM) integration [7], [11], [25], [35], [50], [54] along with emerging circuit technology innovations [25], [43], [47], we propose to replace the single converged GPU that serves both HPC and DL domains with composable, semi-specialized designs as shown in Figures 1(b) and (c).

A COPA-GPU that is specialized for HPC (similar to Figure 1(b)) uses the baseline GPU module (GPM) and a memory system modules providing similar or scaled down capabilities as in the converged GPU today. Augmenting the memory system modules with a very large on-package cache, accessible at high on-package bandwidth and additional off-chip DRAM resources (Figure 1(c)) results in a substantially different COPA-GPU design point that is well suited for bandwidth-hungry DL workloads. This level of specialization is not free, as it requires both intelligent architectural disaggregation of the GPU memory system and employing emerging circuit and packaging techniques. This work aims to shed light on the architectural choices available to designers when building and specializing composable GPU designs.

We make the following contributions:

- We examine historical GPU trends and perform a detailed performance analysis of diverging HPC and DL benchmarks. We show that due to the converged nature of GPUs and future DL scaling requirements, the GPU’s memory bandwidth will become the primary performance bottleneck for GPU based DL training and inference, while being under-utilized for most HPC applications.
- We propose the development of domain-specialized composable GPU architectures. COPA-GPUs provide high levels of GPU design reuse across the HPC and DL

TABLE I: GPU and DL accelerator compute and memory system trends, including a forward-looking GPU projection (GPU-N). We report the attributes of Cerebras as 1/84 tiles in a wafer to provide area-similar comparisons.

GPU Architecture	FP32 [TFLOPS]	FP16 [TFLOPS]	L2 [MB]	-	DRAM BW [GB/s]
NVIDIA P100	11	21	4	-	732
NVIDIA V100	16	125	6	-	900
NVIDIA A100	20	312	40	-	1,555
GPU-N	24	779	60	-	2,687

DL Accelerator	FP32 [TFLOPS]	FP16 [TFLOPS]	On-chip memory [MB]	On-chip memory BW [TB/s]	DRAM BW [GB/s]
Graphcore IPU	31	125	304	45	N/A
Graphcore IPUv2	-	250	900	180	N/A
Cerebras WSE	-	-	214	107	N/A
Groq TSP	-	250	220	80	N/A
Google TPUv2	5	46	37	-	700
Google TPUv3	14	123	37	-	900

domains, while enabling specifically optimized products for each domain. We describe both the architectural modifications, as well as the landscape of technologies, needed to enable COPA-GPUs.

- We evaluate the performance potential of COPA-GPU in the context of DL training and inference and show that very large cache capacity can dramatically improve DL-inference, but both cache and DRAM improvements (available only through COPA designs) are necessary to significantly improve DL-training.
- Finally, we propose a specific COPA-GPU design boosting per-GPU training and inference performance by up to 31% and 35% respectively, while also significantly reducing the cost of scale-out GPU training in datacenters.

II. MOTIVATION AND BACKGROUND

The commercial importance of deep learning is undeniable and numerous companies are now designing targeted DL training and inference accelerators, such as Google’s TPU [33], [34], Graphcore’s IPU [18], Cerebras’ WSE [42], and Groq’s TSP [22]. These application-specific architectures need not maintain a legacy of high performance in other domains, allowing them to make heavily specialized architectural choices compared to GPU architectures that currently serve multiple domains. To better understand the divergence of GPU and DL accelerator design trends we examined recent GPU scaling trends, projected a plausible future GPU configuration, and now compare it to several dedicated DL accelerators.

A. DL Architecture Trends and Projections

Table I summarizes several key compute and memory system characteristics across the three most recent generations of NVIDIA Tesla GPUs targeting both HPC and DL domains. We then forward-project the hardware capabilities of a hypothetical next-GPU configuration (GPU-N) using evolutionary scaling. We calculate the compute and memory bandwidth of GPU-N by linearly extrapolating these parameters from V100 to A100 [59], [61]. We calculate the GPU-N L2 capacity using the lower scaling rate of $1.5\times$ from P100 [58] to V100 (instead of $6.7\times$ from V100 to A100) since GPU-N is highly

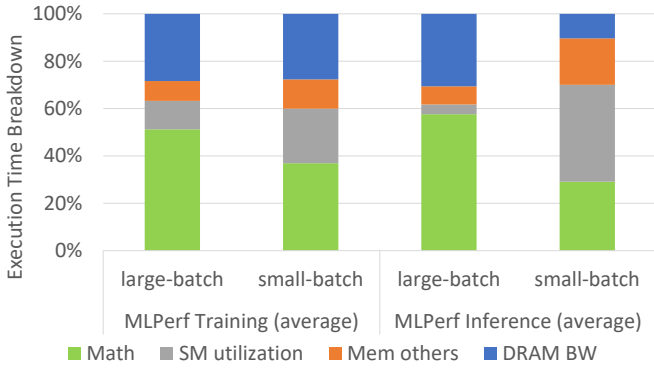


Fig. 2: GPU-N performance bottleneck analysis using the MLPerf DL training and inference suites, for both large-batch and small-batch settings.

unlikely to be able to fit hundreds of MB of SRAM on a single GPU die. Note that we are not trying to accurately project the exact configuration of a future GPU, but rather demonstrate the effect of expected scaling rates on compute and memory bandwidths. Table I makes it clear that while the memory bandwidth to FP32 throughput ratios have generally increased across GPU generations (from $67\times$ in P100 to $112\times$ in GPU-N), the memory bandwidth to FP16 ratio has diminished to only $3.4\times$ in GPU-N.

In addition to several GPU generations, Table I provides attributes of several DL accelerators. The Graphcore, Cerebras, and Groq products all feature very large on-chip SRAMs as main memory, while Google TPUs use off-chip DRAM (HBM). In contrast to GPUs and TPUs, DL accelerators with DRAM-less memory system can provide substantially higher memory bandwidth to FP16 ratios reaching $720\times$ and $320\times$ in IPUv2 and TSP respectively, albeit providing much lower total memory capacity.

B. Diverging DRAM Bandwidth Requirements

To understand the diverging DRAM bandwidth requirements of future GPUs, Figure 2 presents a simulation performance bottleneck analysis of the DL workloads from MLPerf suite (details described later in Section IV-A) for both small- and large-batch scenarios on GPU-N. To correctly identify the source of performance inefficiency, we breakdown the total execution time to individual sets of hardware components, where each bar segment represents the performance overhead introduced by that component during execution. For example, the blue "DRAM BW" bars show the performance overhead attributed to non-ideal DRAM bandwidth, when compared to infinite DRAM bandwidth. Similarly, the orange bars represent the performance penalty caused by all other components in the memory subsystem being non-ideal in terms of bandwidth and latency. The gray bars represent the performance penalty caused by dynamic SM under-utilization (idle SMs) versus an ideal GPU with 100% SM utilization, reflecting inefficiencies such as imperfect work scheduling or lack of sufficient parallelism (sometimes only in phases) within the workload itself.

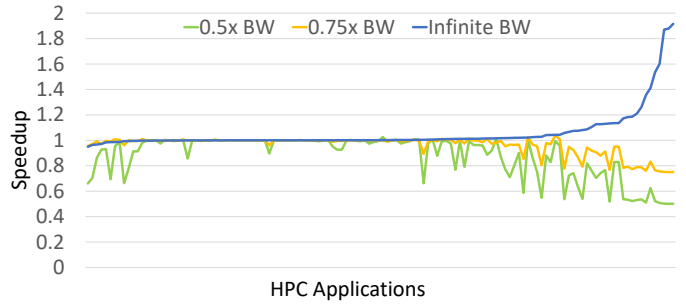


Fig. 3: Performance speedup of various DRAM bandwidth for HPC applications on a GPU-N configuration.

Finally, the green bars show the relative execution time spent in Math units, which should be 100% utilized in the ideal case.

Figure 2 shows that indeed DRAM bandwidth is the primary performance limiter (excluding Math) for DL training in GPU-N, contributing 28% of the total execution time on average across large- and small-batch cases. DRAM bandwidth is also the main performance bottleneck for large-batch DL inference contributing 30% of total execution time. However, at small batch size SM under-utilization accounts for 41% of total execution time and serves as the primary performance bottleneck rather than DRAM bandwidth. This is because MLPerf small-batch inference does not expose enough parallelism to fill an entire GPU that was designed for the datacenter. Moreover, due to small-batch inference's relatively small memory footprints, the majority of each workload's data can be buffered on-chip to avoid DRAM bandwidth to become the bottleneck.

We also simulate the converged GPU-N configuration across varying DRAM bandwidth settings using 130 HPC benchmarks from differing sources including the CORAL [45] and CORAL-2 [46] benchmarks, Amber18 benchmarks [4], FUN3D [55], SPECFEM3D Cartesian [3], GROMACS [1], Laghos [44], and RELION [2]. As shown in Figure 3, in stark contrast to DL applications, most HPC applications are quite insensitive to changes in DRAM bandwidth. When DRAM bandwidth is increased to infinite, a geometric mean speedup of only 5% is achieved. When DRAM bandwidth is decreased, $0.75\times$ BW and $0.5\times$ BW result in 4% and 14% slowdown, respectively. This implies that future increases in DRAM bandwidth will go largely underutilized by most HPC applications if converged GPU designs targeting both DL and HPC domains remain the de facto standard.

C. Very Large Caches for DL-optimized GPUs

Because the memory bandwidth demands of DL applications are likely to exceed what evolutionary DRAM scaling can provide, GPU designers must pursue alternative methods to meet aggressive bandwidth targets. Historically, the GPU's LLC has remained relatively small because HPC workloads have good spatial locality and the majority of the off-chip bandwidth filtering potential can be captured within last level caches that are measured in tens of megabytes. In DL workloads data locality spans multiple temporal and spatial scales, requiring much larger capacities.

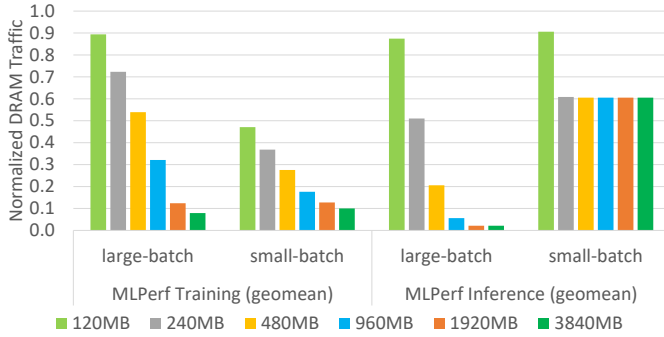


Fig. 4: DRAM traffic reduction versus LLC capacity, normalized to the baseline GPU-N configuration with 60MB of LLC.

To understand how much LLC capacity GPU-N would need to effectively shield the GPU’s DRAM system, we examine the off-chip DRAM traffic reduction achieved when sweeping GPU-N’s LLC capacity from 60MB to 4GB. Figure 4 shows that doubling the LLC capacity to 120MB provides up to 53% reduction in off-chip DRAM traffic in DL training. Further growth to 960MB reduces off-chip BW demand by 82% (5× reduction). We will later show that DRAM traffic reduction from larger caches correlates well with improved training performance. Compared to DL training, large LLC capacities are even more beneficial for DL inference because they enable a larger portion of the workload’s weights and activations to be cached on-chip. For example, in large-batch inference, a 960MB LLC achieves a 16× DRAM traffic reduction, while a 240MB LLC is sufficient to capture all available data reuse data on-chip for small-batch inference because of its smaller memory footprint.

Because modern GPUs are already area limited [7], implementing hundreds of additional megabytes of on-die LLC without severely sacrificing other functionalities is not feasible. Even if it could be done, such an architecture would be out of balance for optimal HPC performance. Because of the different sensitivities to off-chip GPU bandwidth and on-GPU cache capacities between HPC and DL workloads, we now explore the potential benefits of a composable GPU architecture that can satisfy the unique demands of each domain while maximizing design-reuse through a modular on-package design.

III. COMPOSABLE GPU ARCHITECTURE

A COPA-GPU architecture has two primary goals: (i) to largely preserve the existing GPU architecture to minimize design effort and maximize reuse, and (ii) to provide flexibility in specializing the GPU memory system for diverging requirements across application domains. Specifically, we aim to improve the GPU’s memory system with substantially more cache and memory bandwidth than is required for domains such as HPC, to unlock deep learning performance on GPUs. To achieve this range of GPU system capabilities, we leverage on-package multi-chip-module integration to couple a GPU-core die with different memory system dies, each having different allocations of on-package cache and memory resources.

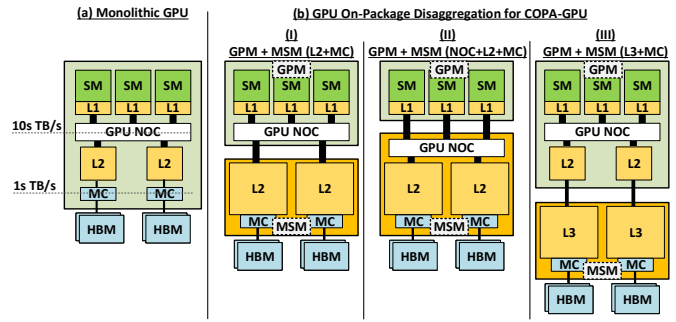


Fig. 5: GPU MCM disaggregation options for practical and composable domain specialization.

A. Practical GPU Disaggregation With COPA-GPU

We propose to disaggregate today’s monolithic GPU into a basic GPU Module (GPM) on-package that is reused without modifications across domain-specialized COPA-GPU instances and a domain-specialized Memory System Module (MSMs) tailored for the specifics of each application domain. The main challenge with on-package disaggregation for GPUs is striking the right balance between the degree of composability and the practicality of effectively shifting the burden of high bandwidth intra-GPU communication from the on-chip to on-package wires.

Figure 5(a) depicts a generic monolithic GPU architecture, with streaming multiprocessors (SMs) and corresponding L1 caches connected to a distributed L2 cache via the GPU network on chip (NoC). L2 cache slices are attached to Memory Controllers (MCs) driving the off-chip DRAM memory interface. While contemporary off-chip DRAM interfaces provide a few TB/s of memory bandwidth (2.7 GB/s in GPU-N), the on-chip interconnects of a modern GPU are designed to transport many tens of TB/s of on-chip bandwidth between the SMs and the on-chip memory hierarchy.

The three possible GPU disaggregation options are shown in Figure 5(b). Option (I) denoted by GPM+MSM(L2+MC) features a GPM containing SMs, L1s, and the GPU NoC, while the MSM includes the L2 cache and the memory controllers. This design can provide more effective die area and die edge than single reticle-limited die to support bigger L2 cache and higher DRAM bandwidth when needed. Option (II) denoted by GPM+MSM(NOC+L2+MC) is similar to (I), but shifts the GPU NoC from the GPM onto the MSM. However, options (I) and (II) are impractical as they both require many tens of TB/s of NoC traffic to instead traverse on-package wires, which Section III-E later shows is not realizable using current or known proposed technologies.

Thus, we choose option (III) denoted by GPM+MSM(L3+MC) for exploring a practical COPA-GPU design as it relies on existing L2 cache bandwidth filtering within the GPM to achieve feasible levels of off-GPM inter-die bandwidth. Additionally, propose to add an additional layer of L3 cache between the L2 cache and MC, and to have both the L3 cache and the MC implemented on the MSM. Such composable design re-organization can

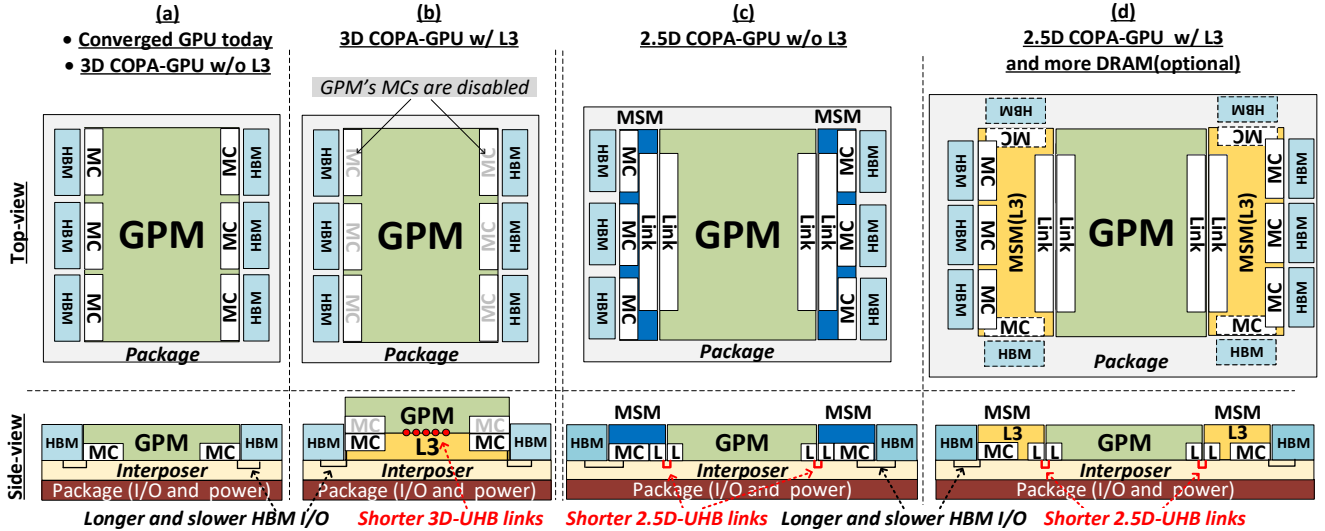


Fig. 6: COPA-GPU architectural options spanning 2.5D and 3D integration domains.

provide more than $4\times$ higher post-L2 bandwidth using previously proposed package integration technologies.

B. COPA-GPU Architectures and Packaging

The architectural domain customization in our proposed COPA-GPU is achieved through integration of a GPM with a dedicated domain-optimized MSM using 2.5D or 3D on-package integration, that could leverage either planar or vertical die stacking approaches. We consider COPA-GPU architectural options spanning both integration strategies while taking into account the unique interdependency between architectural and package technology choices, distilling the advantages and disadvantages of each approach.

Figure 6(a) shows a high-level top and side view of a modern GPU architecture, including a maximum-sized GPU die with the L2 cache and memory controllers on-die and HBM sites attached via 2.5D on-silicon interposer integration. The same diagram shown in Figure 6(a) also describes the basic COPA-GPU GPM, pre-equipped to be 3D integrated with an MSM die to provide a 3D DL-optimized COPA-GPU variant.

Figure 6(b) illustrates a 3D organization of a DL-optimized COPA-GPU where the GPM die from Figure 6(a) is integrated with an MSM carrying additional L3 cache. The MSM is vertically attached via a 3D ultra-high bandwidth (3D-UHB) link using high-density intra-die bonding, with up to 14.7 TB/s of bandwidth, further detailed in Section III-E. The MSM is positioned between the GPU and silicon interposer, and provides all the essential connectivity between the GPM and the silicon interposer via through silicon vias (TSVs), as shown in Figure 6(b:side-view). The composable nature of a 3D COPA-GPU allows for designs both with (for DL) and without (for HPC) additional L3. The primary disadvantage of a 3D COPA-GPU organization is that it cannot provide any additional die edge to improve DRAM scaling.

Figure 6(c) shows a basic 2.5D COPA-GPU integrating a GPM with up to two MSM modules in a 2.5D organization targeting HPC. The design of a 2.5D COPA-GPU retains most of its original functionality on the base GPM but offloads the memory controllers (MC) and HBM I/O to new (small) in-package MSMs. A 2.5D COPA-GPU has the advantage that offloading of GPM area allocated to MC and HBM I/O frees up die area for the implementation of UHB links and additional compute resources in the baseline COPA-GPU.

Figure 6(d) augments the 2.5D COPA-GPU in Figure 6(c) with a large L3 cache and additional DRAM stacks, subject to package area limitations. The same GPM die is reused between Figure 6(c) and (d) and this 2.5D DL-optimized organization has several advantages compared to a 3D organization. First, it can provide up to $2\times$ more L3 capacity than the 3D organization. Second, the additional MSM geometry increases the total available die-edge of the design. This die-edge can provide up to $1.7\times$ or $2.3\times$ higher HBM BW and larger capacity, via 10 total HBM sites, or 14 total HBM sites using maximally sized MSMs (not shown).

C. COPA-GPU Microarchitectures

Figure 7 presents the microarchitecture of the proposed memory systems for both the 3D and 2.5D COPA-GPU designs. Figures 7(a) and (b) outline the main components of a 3D COPA-GPU with and without an extended L3 MSM. The most significant difference between current GPU architectures and the 3D COPA-GPU is the addition of a new switching component that steers requests from the L2 to the on-chip memory controller or to the UHB links, depending on whether the MSM is present in-package.

If the MSM is not present (Figure 7(a)), the switch is configured to steer the memory requests directly from the L2 to its local MC, similarly to today's GPUs. If the MSM is present, (Figure 7(b)), the switch is reconfigured to steer post-L2 traffic to the L3 via the UHB link. This design requires

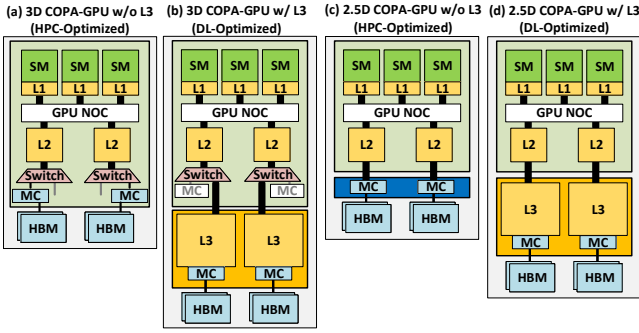


Fig. 7: L3 cache microarchitecture in COPA-GPU designs.

the MSM to implement its own MC that connects to HBM I/O, with silicon area overheads stemming from adding the UHB link, the TSV-based I/O, and power delivery between GPM and the silicon interposer dies. In the 2.5D COPA-GPU designs without and with additional L3 capacity on the MSM (Figures 7(c) and (d)), the GPM is completely stripped of its original MC and HBM I/O, and post-L2 traffic is always routed to the MSM modules over on-package UHB links. Both the 2.5D COPA-GPU configurations consist of the same GPM, but are equipped with different versions of the MSM to serve different application classes (i.e. with or without L3 and additional HBM sites).

In both designs, the L3 cache is architecturally implemented as yet another level of memory-side cache that (when present) backs the existing L2. It is neither inclusive nor exclusive, nor does it require coherence with the L2 because the L2 already serves as the point of coherence in GPU systems. Lines present in the L2 always supercede lines in the L3 from the GPU’s perspective and are written back to the L3 upon eviction from the L2. No requests are routed to the L3 without first being serviced at the L2.

D. Costs and Benefits of the COPA-GPU

The major drawback of a 2.5D COPA-GPU organization is that it increases the package size. Whereas the 3D COPA organization has minimal impact on package complexity (same top view), but the base GPM must account for the implementation of the distributed on-die UHB link bonding used for vertical inter-die communication (Section III-E) and the TSVs overheads used for traversing through the MSM die. We estimate that in the 3D case, the cost of providing as much as 14.7 TB/s bandwidth of UHB I/O will consume less than 4% of silicon surface and metal layers for inter-die communication bonding. The majority of the active area and lower-level metals under the 3D bonding can likely be reused for other logic in the GPM. In 2.5D designs, the maximally sized links results in approximately 6% area overheads assuming a 20Gbps signaling rate. Section III-E provides further details on these assumptions.

Even though the COPA-GPU approach introduces 4%-6% area overhead due to new MCM communication interfaces, this area (and thus cost overhead) will be more than offset by the savings in the HPC oriented variants by not carrying

TABLE II: Bandwidth and energy characteristics assumptions for 2.5D and 3D ultra-high bandwidth (UHB) in this work.

Technology	BW Density	Max Bisection BW	Energy/bit
2.5D	256GB/s/mm	14.7TB	0.3 pJ/b
3D	512GB/s/mm ²	>14.7TB	0.05 pJ/b

forward the unnecessary and expensive DL-oriented memory subsystem. Moreover, we believe that in the future even non-composable GPU designs will turn to MCM organizations due to looming reticle limitations, effectively introducing similar MCM link overheads into *all* GPU designs.

Adding new communication interfaces that memory system requests must traverse comes with an additional energy tax. We estimate that the 2.5D organized UHB-link consumes less than 9 Watts, assuming peak 100% bandwidth utilization at 0.3pJ/b with a 25% wire toggle-rate. The 3D link consumes less than 2 watts, due to its more efficient link technology and overall shorter communication distances (Section III-E).

A large L3 reduces the number of DRAM accesses, more than offsetting the additional cost of the UHB link traversal and L3 accesses. Figure 4 shows that the 960MB and 1.9GB L3 configurations reduce overall DRAM traffic by up to 94% and 98%, respectively. We estimate that fetching a cache line from an SRAM-based COPA-GPU L3 into the GPM will consume approximately 4× less energy than accessing HBM memories. These estimates fully account for the energy associated with traveling to an SRAM sub-array on a MSM-die and back, as well as the energy consumed by the SRAM sub-array [8], [10], [37], [72]. Consequently, we estimate that either COPA-GPU design (utilizing a 960MB L3 cache) will reduce the total HBM-related GPU energy consumption by up to 3.4×. While left for future exploration, the cost of the MSM caching modules could be reduced by implementing them in older and less expensive processes.

E. COPA-GPU Enabling Technologies

The feasibility of COPA-GPUs depends on several technologies reaching maturity for industrial implementation.

Cache Technology Projections: Large caches can be realized through high density Embedded DRAM (eDRAM) [9] or SRAM technologies [12], [21]. IBM recently implemented a 960MB cache on a 696mm² die using a 14nm eDRAM technology [9]. Graphcore’s recently announced second-generation IPU [18] integrates 900MB of SRAM along with thousands of cores on a single 823 mm² die using TSMC’s 7nm process. Cache density is dictated by combination of the bitcell area, control overheads, and the bandwidth requirements. Because the COPA-GPU’s L3 is designed to provide lower bandwidth than L2, we estimate that a future reticle limited 826 mm² MSM die (the same die size as an NVIDIA A100 GPU [61]), can provide up to 2GB of L3 cache. Though, the remainder of this work assumes a conservative projection of a 960MB L3 on an 826mm² die, which implies a maximum of 960MB L3 in a 3D COPA-GPU with single MSM die and 1920MB L3 in a 2.5D COPA-GPU with two MSM dies.

TABLE III: MLPerf training and inference benchmarks.

Benchmark	Type	Small-batch		Large-batch	
		Per-GPU batch size	Memory footprint	Per-GPU batch size	Memory footprint
resnet	training	12	989MB	128	6GB
ssd	training	4	559MB	128	7.9GB
maskrcnn	training	1	2.1GB	6	9.9GB
minigo	training	128	105MB	2,048	1.5GB
gnmt	training	32	3GB	256	8.3GB
transformer	training	640	4.5GB	5120	7.9GB
ncf	training	65,526	657MB	1,048,576	4.5GB
resnet	inference	1	49MB	232	1.1GB
mobilenet	inference	1	16MB	704	2GB
ssd-small	inference	1	24MB	288	2GB
ssd-large	inference	1	136MB	6	562MB
gnmt	inference	1	300MB	128	961MB

High Bandwidth 2.5D and 3D Interconnects: High-speed links that enable 2.5D integration are rapidly maturing [16], [19], [43], [71]. Chen et al. [16] recently demonstrated 20Gbps signaling rates across a 2.5mm silicon interposer layer at 0.3pJ/b, resulting in a $\sim 200\text{GB/s/mm}$ bandwidth density per layer, which can be further increased at shorter distances. This work assumes a 2.5D COPA-GPU UHB link with a bandwidth density of 256GB/s/mm , thus the dedicated edges of the 826mm^2 GPM module can provide up to 14.7TB/s of off-GPM bandwidth as described in Figure 6(d). While this bandwidth to the MSM far exceeds the actual L3 bandwidth requirement, it provides headroom for future increases in off-die communication.

3D integration is also maturing [13], [26], [28], [30], [74]. For example, TSMC’s System on Integrated Chips (SoIC) is expected to provide ultra-dense 3D interconnects [13], [26] with greater than 1TB/s/mm^2 of inter-die bandwidth, assuming a 1 Gbps signaling rate. We conservatively assume 3D-UHB links with 512GB/s/mm^2 of bandwidth density at 0.05 pJ/b. Achieving the assumed 14.7TB/s of data bandwidth for a 2.5D COPA-GPU would require 28.7mm^2 (less than 4%) of silicon area for the inter-die communication bonding. Table II summarizes the UHB link characteristics for both 2.5D and 3D scenarios.

IV. EVALUATION

We now present our simulation methodology, examine the performance sensitivity of the baseline COPA-GPU architecture to DRAM bandwidth and on-package LLC capacity, and evaluate several specific DL-specialized COPA-GPU configurations in both training and inference scenarios.

A. Methodology

To provide performance projections for DL workloads, we perform our studies using unmodified workloads from the MLPerf training and inference benchmark suites [48], [65] for one end-to-end iteration of the workloads, rather than using disjoint and isolated GPU kernel calls. This approach allows us to characterize the overall throughput and capture a new important class of inter-kernel data reuse that will drive future memory system design on GPUs. MLPerf is the de

TABLE IV: Detailed GPU configurations.

Configuration	NVIDIA V100	NVIDIA A100	GPU-N
SMs	80	108	134
GPU frequency (GHz)	1.4	1.4	1.4
FP32 (TFLOPS)	15.7	19.5	24.2
FP16 (TFLOPS)	125	312	779
L2 cache (MB)	6	40	60
DRAM BW (GB/s)	900	1,555	2,687
DRAM Capacity (GB)	16	40	100

facto standard for DL benchmarking and is maintained by major DL chip vendors including NVIDIA, Google, and Intel. Table III shows the seven MLPerf training benchmarks and the five inference benchmarks used, taken from NVIDIA’s publicly available MLPerf training v0.6 and MLPerf inference v0.5 submissions [51], [52]. These codes are highly optimized for NVIDIA GPUs by exploiting high-throughput Tensor Cores [59] and have demonstrated performance scalability from a single to thousands of GPUs.

To build a complete picture of future deep learning scenarios, we run all our DL benchmarks in two different configurations. For DL training, we use a large per-GPU batch size to characterize a single-GPU training situation and a small per-GPU batch size to represent a large-scale training system. For DL inference, we use a large per-GPU batch size to represent a datacenter processing inference task with large numbers of concurrent queries and a small per-GPU batch size for an edge-device scenario with real-time processing requirements. Although small-batch inference workloads do not commonly run on the large datacenter-grade GPUs we evaluate in this paper, we include them in our studies for completeness as future GPU designs could also be scaled down (in aggregate) to build niche-specific GPU products in traditional or COPA-GPU form.

The batch sizes we choose for each scenario are taken from NVIDIA’s MLPerf submissions and are shown in Table III. For our evaluations, we execute each application on a single NVIDIA Tesla V100 and collect a GPU execution trace from a full end-to-end iteration. We focus on the per-GPU workload analysis and omit the all-reduce synchronization overheads when projecting performance for large-scale DL training. All-reduce performance largely depends on the implementation of the inter-GPU network, which is beyond the scope of this work but is also receiving attention within the architecture community [39], [41].

We simulate these workloads using a trace based, partially execution driven, architectural-level GPU simulator using methodology similar to that of NVIDIA’s NVArchSim [73] and AccelSim [38]. Our simulator provides very fast simulation of deterministic portions of an application without sacrificing simulation accuracy or correctness during non-deterministic application phases. Our simulator has been correlated to NVIDIA Tesla V100 GPU using hundreds of HPC and ML/DL workloads and achieves a 0.986 Pearson correlation to real hardware.

Our analysis focuses on the projected GPU-N configuration

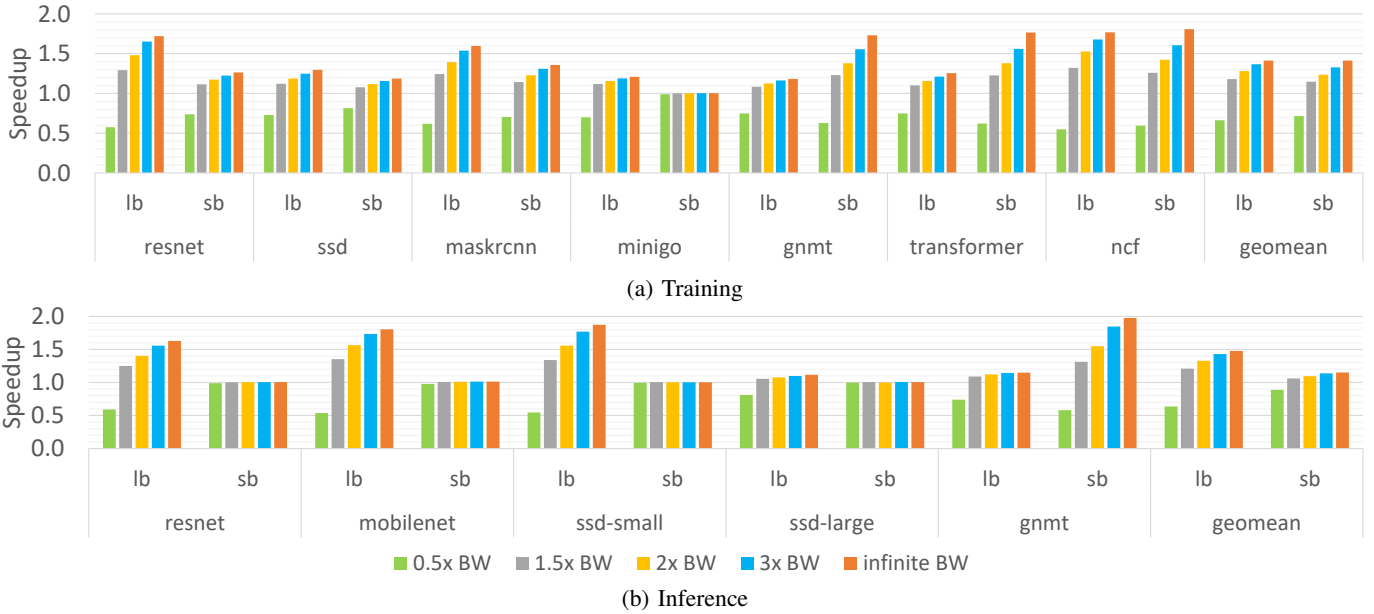


Fig. 8: Performance of a basic COPA-GPU with varying DRAM bandwidth for large-batch (*lb*) and small-batch (*sb*) settings, normalized to the baseline GPU-N performance.

described in Table IV. GPU-N’s SM count growth beyond NVIDIA A100’s is proportional to the projected FP32 throughput (from Table I) with a constant SM frequency. GPU-N’s DRAM capacity is projected based on a linear extrapolation similar to the projections done for the DRAM bandwidth.

B. DL Performance Sensitivity to DRAM Bandwidth

We perform a detailed sweep of the DRAM bandwidth settings for the basic COPA-GPU design without L3 (similar to GPU-N) from half of its nominal bandwidth (1.3TB/s) up through infinite bandwidth. Figure 8 summarizes the overall performance normalized to the 2.7TB/s baseline. Workload performance scales steadily with growing DRAM bandwidth up to a $3\times$ BW (8.1TB/s) setting in most of the training and inference scenarios, with diminishing returns beyond this point. Small-batch inference applications are less sensitive to DRAM bandwidth due to their relatively small footprint (more details in Section IV-C), while the remaining DL training and inference workloads show that even a relatively modest $1.5\times$ increase in DRAM bandwidth from 2.7TB/s to 4TB/s would lead to notable speedups of up to 18% for training and 21% for inference.

From these results we conclude that modern GPUs are on track to be severely DRAM bandwidth limited and that additional raw DRAM bandwidth is the most powerful tool for scaling DL performance. However, because evolutionary improvement in HBM memory frequency and pin density is unlikely to provide a substantially higher bandwidth scaling ratio than our aggressively projected $1.7\times$ (for GPU-N), we explore the potential of a very large and high bandwidth on-package cache to close this gap in future COPA-GPUs.

C. DL Performance Sensitivity to Cache Capacity

To understand the impact of large caches on DRAM bandwidth reduction in future GPUs, we sweep the LLC (L2) cache

capacity of the basic COPA-GPU without L3 from 60MB to 3,840MB to characterize the performance potential of the larger on-package caches. A perfect L2 where all requests hit in the L2 caches serves as the upper bound on performance. Figure 9 shows the performance of these different L2 configurations, normalized to the 60MB baseline. Increasing the L2 capacity results in performance gain equivalent to large increases in DRAM bandwidth, primarily because of the significant off-chip DRAM traffic reduction, as shown in Figure 4.

For DL training, 480MB of L2 performs slightly worse than a $1.5\times$ increase in DRAM bandwidth and 960MB of L2 performs slightly worse than a $2\times$ increase in DRAM bandwidth (comparing to Figure 8). Yet larger L2 caches continue to incrementally improve the performance, but even a 3,840MB L2 still results in an 8% and 13% performance gap in large-batch and small-batch DL training workloads when compared to a perfect L2. Because DL inference applications generally have smaller memory footprint sizes than DL training, performance saturates once all workload data can be cached. The saturation points are 1,920MB and 240MB for large- and for small-batch inference respectively, which correspond to their memory footprints listed in Table III.

We conclude that a substantially larger LLC is an attractive solution for scaling DL performance within a COPA-GPU, however closing the performance gap to a perfect L2 would require 4GB of on-package cache, which is impractical even under aggressive technology projections. As a result, to maximize DL performance COPA-GPUs must not just utilize a very large L3 cache, but combine a large L3 and higher DRAM bandwidth made available with additional MSM-die edge in a 2.5D COPA-GPU design.

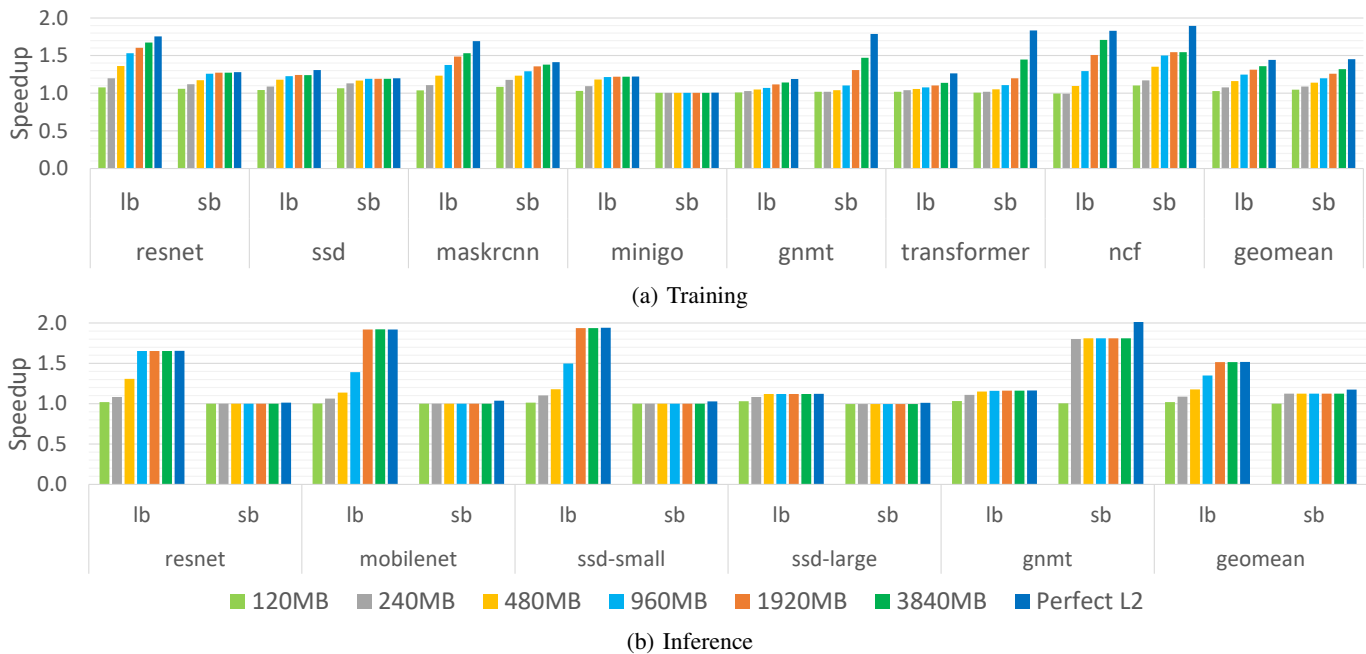


Fig. 9: Performance of a basic COPA-GPU with varying LLC capacities for both large-batch (*lb*) and small-batch (*sb*) settings, normalized to the baseline GPU-N performance.

TABLE V: COPA-GPU architectural parameters.

Architecture configuration	LLC capacity (MB)	DRAM BW (TB/s)	DRAM capacity (GB)
GPU-N	60	2.7	100
HBM+L3	960	2.7	100
HBML+L3	960	4.5	167
HBM+L3L	1920	2.7	100
HBML+L3L	1920	4.5	167
HBMLL+L3L	1920	6.3	233
Perfect L2	infinite	infinite	infinite

D. DL Performance Scaling with COPA-GPU

Table V summarizes the DL-optimized COPA-GPU configurations that are enabled by architectural choices outlined in Section III. The HBM+L3 design provides 960MB of L3 cache through either 3D stacking with a single maximum sized MSM die, or 2.5D stacking with two MSM dies, each set to half of the maximum die size. The option with more HBM resources, denoted by an HBML in the HBML+L3, applies only to 2.5D, by exploiting the extra MSM die edge area to provide a $1.7\times$ higher HBM bandwidth and a larger HBM capacity (10 HBM sites in total). With two maximally-sized MSM dies in 2.5D stacking scenario, the L3 cache capacity and the additional DRAM bandwidth can be scaled to up to 1,920MB and $2.3\times$ of the baseline DRAM bandwidth (via 14 HBM sites) respectively. As a result, we consider three additional COPA-GPU configurations with 1,920MB of L3 cache and varying HBM resources: HBM+L3L, HBML+L3L and HBMLL+L3L, with 2.7TB/s, 4.5TB/s and 6.3TB/s of DRAM bandwidth, respectively.

Before moving to overall results, we first analyze the UHB on-package link bandwidth requirements by sweeping the



Fig. 10: Performance of a HBM+L3 COPA-GPU with varying UHB link bandwidth to the L3 cache, normalized to the baseline GPU-N performance.

unidirectional L3 bandwidth in the HBM+L3 configuration with half of its baseline DRAM bandwidth ($0.5\times RD + 0.5\times WR$ which sums to 2.7TB/s) up through infinite bandwidth. Figure 10 summarizes the geometric mean speedup of the MLPerf applications (training and inference), normalized to the baseline GPU-N (without L3). The performance increases substantially when the L3 bandwidth grows from $0.5\times RD + 0.5\times WR$ to $2\times RD + 2\times WR$, with diminishing returns beyond that point. Overall, the UHB bandwidth configurations of $2\times RD + 2\times WR$ (total 10.8TB/s) comes within 3% and 6% of the unlimited bandwidth settings for training and inference respectively. This bandwidth is well within the capabilities of next generation 2.5/3D interconnect technologies assumed in our designs.

We also evaluate the effect of the UHB link latency by varying the total round-trip latency between the L2 and L3 caches from $0.25\times$ to $1\times$ of the DRAM access latency. Our experiments (not shown) indicate that COPA-GPU architecture is not sensitive to L3 latency, as performance changes by less

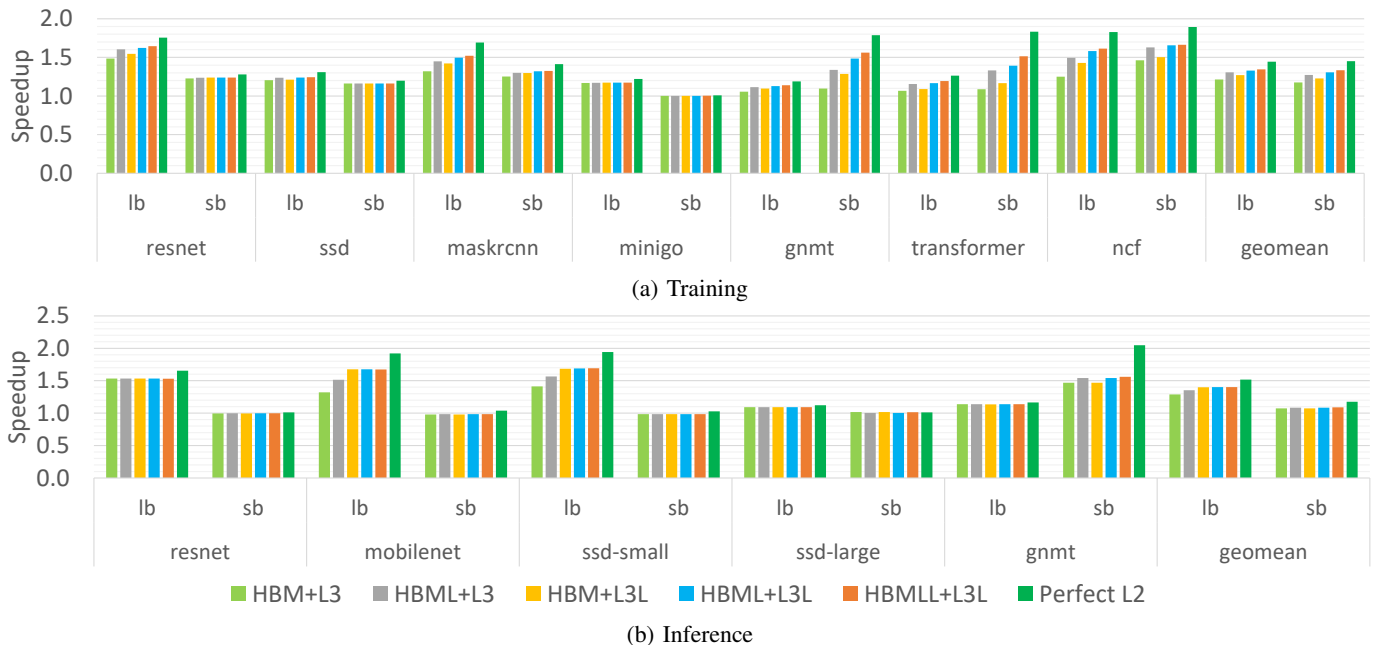


Fig. 11: Performance of DL-optimized COPA-GPUs with varying designs, normalized to the baseline GPU-N performance. Large-batch and small-batch cases are denoted by *lb* and *sb*.

than 2% across this latency range. As a result, we set the UHB link bandwidth to be $2 \times RD + 2 \times WR$, for a total of 10.8TB/s and the round-trip latency between L2 and L3 (UHB link latency plus L3 access latency) to be half of the DRAM access latency for all the COPA-GPU configurations with L3 that are listed in Table V.

Figure 11 summarizes the MLPerf training and inference performance of the COPA-GPU designs from Table V in large batch (*lb*) and small batch (*sb*) settings. Unsurprisingly, larger cache capacity and higher memory bandwidth universally improve both large-batch and small-batch training performance. For example, the additional cache capacity in HBM+L3 improves large-batch and small-batch performance by 21% and 18% respectively, making it an attractive 3D COPA-GPU design. Further, the additional HBM bandwidth provided by the HBML+L3 configuration achieves an overall 31% and 27% speedup, making it an attractive 2.5D COPA-GPU design choice. HBM+L3L doubles L3 capacity instead of scaling DRAM bandwidth and results in lower speedups than HBML+L3 (by 4%) at both large- and small-batch scenarios, indicating that increasing L3 capacity alone is not the best solution to scaling training. Finally, ambitious DRAM options such as HBML+L3L and HBMLL+L3L result in marginal performance gains (4%) when compared to HBML+L3 and do not justify its additional cost.

For large-batch inference, the large L3 capacity in HBM+L3 improves the performance by 29% and HBM+L3L can reach speedup as high as 40%. With 1,920MB of L3, further increases in HBM bandwidth is not beneficial because most of the DRAM traffic has already been filtered out by the large L3 cache. In fact, though not shown, we find that DRAM bandwidth could be even reduced by 50% without

affecting the performance. For small-batch inference, because the performance saturation point is at 240MB of LLC, the performance improvement via the combination of L3 and HBM is just 9%.

Overall, we conclude that HBML+L3, which combines a substantially larger L3 cache (960MB) and moderately higher DRAM bandwidth (4.5 TB/s), is likely the most optimal COPA-GPU design that will perform well for both DL training (with 31% gain at large-batch and 27% gain at small-batch) and inference (with 35% gain at large-batch and 8% gain at small-batch) without adding significant unnecessary cost through overprovisioning of memory resources. Inference is more sensitive to cache capacity and less sensitive to DRAM bandwidth than DL training, and trading off additional HBM resources for increased LLC capacity could be a plausible strategy if designing a COPA-GPU specialized for just DL inference.

A large COPA-GPU enabled L3 reduces the total DRAM-related per-GPU energy consumption by up to $3.4\times$, as shown in Section III-C. However, the improved DL-optimized COPA-GPU utilization may lead to increased total design power that may not be entirely mitigated by the power reduction within the memory system. To mitigate growing thermal density, we expect future high-end GPU systems will rely on liquid cooling technologies to enable increased thermal envelopes compared to those possible today [15], [62].

E. COPA-GPU Training Cost Efficiency at Scale

At scale, multi-GPU training performance is eventually limited by decreasing per-GPU compute efficiency and growing system-level synchronization overheads. To understand the scale-out efficiency of DL-optimized COPA-GPUs, we

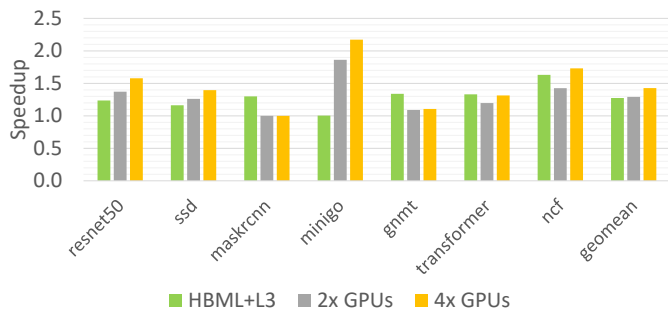


Fig. 12: Performance of DL-optimized HBML+L3 COPA-GPUs versus additional data parallelism via 2×GPU-Ns and 4×GPU-Ns, normalized to the baseline GPU-N performance.

compare the performance of an HBML+L3 COPA-GPU based system with 2× and 4× larger systems comprising the baseline GPU-Ns. We fix the global batch size across all configurations to maintain the same statistical efficiency [63]. Consequently, the per-GPU batch size drops to one half and one quarter for the baseline GPU-N configurations. We do not extrapolate the additional overheads of distributed gradient synchronization at larger scales, and thus our analysis favors the 2× and 4× GPU-N configurations.

Figure 12 shows that doubling and quadrupling the number of baseline GPU-N instances (2× GPU-Ns and 4× GPU-Ns) results in mean 29% and 43% performance gains respectively for our training workloads. We find that a DL-optimized HBML+L3 COPA-GPU configuration (with 27% performance gain) provides similar levels of performance to 2× GPU-Ns, yet should cost significantly less than buying and hosting 2× larger installations of traditional GPU-Ns. When compared to GPU-N, even though HBML+L3 doubles the area by adding close to 826mm² of silicon, it is dominated by regular SRAM cache arrays that are expected to achieve high manufacturing yields due to built-in redundancy and error recovery. Moreover, this aggregate area is split into two smaller dies, resulting in substantially lower cost per mm². HBML+L3 integrates 1.6× more HBM memory, resulting in total aggregate cost lower than 2× of GPU-N. Thus, DL-optimized COPA-GPUs will provide substantially better cost-performance at scale, saving on not just overall GPU cost but additional system-level collateral such as datacenter floorspace, CPUs, network switches, and other peripheral devices.

V. RELATED WORK

Leveraging high capacity and high bandwidth on-chip and on-wafer caches, or scratch memories, to store DL weights and activations has been well explored for DL training/inference architectures. DaDianNao [14] was designed with 36MB of on-chip eDRAM to cache model weights. Google’s TPUv1 [34] allocated 28MB of on-chip memory mostly for caching activations, while TPUv2 and TPUv3 [33] increased it to 37MB. Recent DL accelerators such as Graphcore’s IPU [18], Groq’s TSP [22], Alibaba’s HanGuang [32], and Cerebras’s WSE [42] replaced off-chip memory with hundreds of MBs of high-bandwidth on-chip SRAM to satisfy

increasing memory bandwidth requirements. Unlike domain specific accelerators that are highly tuned for DL workloads, COPA-GPUs provide high levels of GPU design reuse across application domains, while also enabling memory-system specialization for individual domains.

Multi-chip module (MCM) packaging has been extensively studied and deployed to integrate heterogeneous and homogeneous chips within a package, aiding the scaling of compute and memory bandwidths for a wide variety of legacy GPU and CPU applications. Prior work [7], [8], [50] has focused on developing MCM-GPU architectures to strong scale GPU performance beyond the limitations of a single monolithic die by leveraging on-package and on-board integration technologies. In a follow-on work [66], [75], the authors extend MCM-GPU architectures with advanced caching and HW/SW cache-coherency protocols to overcome NUMA limitations. MCM-3D-NoC [64] tackled the interconnect scalability issues of MCM integration over active interposers. In the CPU space, recent AMD CPU architectures [11], [54] leverage multi-module on-board integration to provide scalable and modular CPU architectures. Finally, Kannan et al. [35] proposed to disaggregate large monolithic CPU designs into smaller chips for cost reduction. In [69], the authors propose and quantify the costs and benefits of using MCMs with fine-grained domain specific chiplets for DL inference.

General purpose CPU SoCs have already leveraged MCM designs with very large on-package eDRAM caches. Intel improved its mobile CPU performance by combining a CPU SoC and 128MB of on-package eDRAM organized as a victim cache [29] and IBM scaled up its Gen-Z mainframe performance with 960MB of L4 eDRAM cache [9]. While a COPA-GPU leverages the previously proposed concepts of on-package integration and large caches, our work is (1) the first to identify and solve the diverging architectural requirements between FP32 (or larger) based HPC and FP16 (or smaller) based DL workloads in GPUs and (2) the first to develop the reusable GPU architecture concept, enabling cost-effective GPU domain-specialization for HPC and deep learning.

VI. CONCLUSION

In this work, we demonstrate that diverging architectural requirements between the HPC and DL application domains put converged GPU designs on a trajectory to become significantly under-provisioned for DL and over-provisioned for HPC. We propose a new composable GPU architecture that leverages emerging circuit and packaging technologies to provide specialization, while maintaining substantial compatibility across product lines. We demonstrate that COPA-GPU architectures can enable selective deployment of on-package cache and off-chip DRAM resources, allowing manufacturers to easily tailor designs to individual domains. Our analysis shows that DL-optimized COPA-GPUs will provide impressive per-GPU training and inference performance improvements, while still efficiently supporting scaled-down HPC-targeted designs. DL-optimized COPA-GPUs will also result in reduced cost datacenter cost by minimizing the number of GPUs required

to achieve scale-out training performance targets, making COPA-GPU an attractive paradigm for increasing individual and aggregate GPU performance without over-optimizing the product for any specific domain.

REFERENCES

- [1] "GROMACS." [Online]. Available: <http://www.gromacs.org/>
- [2] "RELION." [Online]. Available: <https://github.com/3dem/relion>
- [3] "SPECFEM3D Cartesian." [Online]. Available: <https://geodynamics.org/cig/software/specfem3d/>
- [4] "The Amber18 Benchmarks," 2018. [Online]. Available: <http://ambermd.org/>
- [5] "AMD INSTINCT™ MI100 ACCELERATOR." 2020. [Online]. Available: <https://www.amd.com/system/files/documents/instinct-mi100-brochure.pdf>
- [6] D. Amodei, S. Ananthanarayanan, R. Anubhai, J. Bai, E. Battenberg, C. Case, J. Casper, B. Catanzaro, Q. Cheng, G. Chen, J. Chen, J. Chen, Z. Chen, M. Chrzanowski, A. Coates, G. Diamos, K. Ding, N. Du, E. Elsen, J. Engel, W. Fang, L. Fan, C. Fougner, L. Gao, C. Gong, A. Hannun, T. Han, L. Johannes, B. Jiang, C. Ju, B. Jun, P. LeGresley, L. Lin, J. Liu, Y. Liu, W. Li, X. Li, D. Ma, S. Narang, A. Ng, S. Ozair, Y. Peng, R. Prenger, S. Qian, Z. Quan, J. Raiman, V. Rao, S. Satheesh, D. Seetapun, S. Sengupta, K. Srinet, A. Sriram, H. Tang, L. Tang, C. Wang, J. Wang, K. Wang, Y. Wang, Z. Wang, Z. Wang, S. Wu, L. Wei, B. Xiao, W. Xie, Y. Xie, D. Yogatama, B. Yuan, J. Zhan, and Z. Zhu, "Deep Speech 2 : End-to-End Speech Recognition in English and Mandarin." in *ProInternational Conference on Machine Learning (ICML)*, 2016.
- [7] A. Arunkumar, E. Bolotin, B. Cho, U. Milic, E. Ebrahimi, O. Villa, A. Jaleel, C.-J. Wu, and D. Nellans, "MCM-GPU: Multi-Chip-Module GPUs for Continued Performance Scalability," in *International Symposium on Computer Architecture (ISCA)*, 2017.
- [8] A. Arunkumar, E. Bolotin, D. Nellans, and C.-J. Wu, "Understanding the Future of Energy Efficiency in Multi-Module GPUs," in *International Symposium on High-Performance Computer Architecture (HPCA)*, 2019.
- [9] C. Berry, B. Bell, A. Jatkowski, J. Surprise, J. Isakson, O. Geva, B. Deskin, M. Cichanowski, D. Hamid, C. Cavitt, G. Fredeman, A. Saporito, A. Mishra, A. Buyuktosunoglu, T. Weibel, P. Lobo, P. Parashurama, R. Bertran, D. Chidambarrao, D. Wolpert, and B. Bruen, "IBM z15: A 12-Core 5.2GHz Microprocessor," in *International Solid-State Circuits Conference (ISSCC)*, 2020.
- [10] E. Bolotin, D. Nellans, O. Villa, M. O'Connor, A. Ramirez, and S. Keckler, "Designing Efficient Heterogeneous Memory Architectures," *IEEE Micro*, vol. 35, no. 4, 2015.
- [11] T. Burd, N. Beck, S. White, M. Paraschou, N. Kalyanasundharam, G. Donley, A. Smith, L. Hewitt, and S. Naffziger, "'Zeppelin': An SoC for Multichip Architectures," *IEEE Journal of Solid-State Circuits*, vol. 54, no. 1, January 2019.
- [12] J. Chang, Y. Chen, G. Chan, H. Cheng, P. Wang, Y. Lin, H. Fujiwara, R. Lee, H. Liao, P. Wang, G. Yeap, and Q. Li, "A 5nm 135Mb SRAM in EUV and High-Mobility-Channel FinFET Technology with Metal Coupling and Charge-Sharing Write-Assist Circuitry Schemes for High-Density and Low-VMIN Applications," in *International Solid-State Circuits Conference (ISSCC)*, 2020.
- [13] M. Chen, F. Chen, W. Chiou, and D. C. H. Yu, "System on Integrated Chips (SoIC) for 3D Heterogeneous Integration," in *Electronic Components and Technology Conference (ECTC)*, 2019.
- [14] Y. Chen, T. Luo, S. Liu, S. Zhang, L. He, J. Wang, L. Li, T. Chen, Z. Xu, N. Sun, and O. Temam, "DaDianNao: A Machine-Learning Supercomputer," in *International Symposium on Microarchitecture (MICRO)*, 2014.
- [15] "Google Brings Liquid Cooling to Data Centers to Cool Latest AI Chips," 2018. [Online]. Available: <https://www.datacenterknowledge.com/google-alphabet/google-brings-liquid-cooling-data-centers-cool-latest-ai-chips>
- [16] B. Dehlaghi, N. Wary, and T. Carusone, "Ultra-Short-Reach Interconnects for Die-to-Die Links: Global Bandwidth Demands in Microcosm," *IEEE Solid-State Circuits Magazine*, vol. 11, no. 2, 2019.
- [17] J. Devlin, M.-W. Chang, K. Lee, and K. Toutanova, "BERT: Pre-training of Deep Bidirectional Transformers for Language Understanding," in *arXiv preprint arXiv:1810.04805*, 2018.
- [18] "Graphcore IPU." 2020. [Online]. Available: <https://www.graphcore.ai/products/ipu>
- [19] D. Greenhill, R. Ho, D. Lewis, H. Schmit, K. Chan, S. Satsat, D. How, P. McElheny, K. Duwel, J. Schulz, D. Faulkner, G. Iyer, G. Chen, H. Phoon, H. Lim, W.-Y. Koay, and T. Garibay, "A 14nm 1GHz FPGA with 2.5D Transceiver Integration," in *International Solid-State Circuits Conference (ISSCC)*, 2017.
- [20] S. Gu, E. Holly, T. Lillicrap, and S. Levine, "Deep Reinforcement Learning for Robotic Manipulation with Asynchronous Off-Policy Updates," in *International Conference on Robotics and Automation (ICRA)*, 2017.
- [21] Z. Guo, D. Kim, S. Nalam, J. Wiedemer, X. Wang, and E. Karl, "A 23.6-Mb/mm2 SRAM in 10-nm FinFET Technology With Pulsed-pMOS TVC and Stepped-WL for Low-Voltage Applications," in *International Solid-State Circuits Conference (ISSCC)*, 2018.
- [22] L. Gwennap, "Groq Rocks Neural Networks," in *Microprocessor Report by the Linley Group*, 2020.
- [23] K. He, X. Zhang, S. Ren, and J. Sun, "Deep Residual Learning for Image Recognition," in *Conference on Computer Vision and Pattern Recognition (CVPR)*, June 2016.
- [24] X. He, L. Liao, H. Zhang, L. Nie, X. Hu, and T.-S. Chua, "Neural Collaborative Filtering," in *International World Wide Web Conference (WWW)*, 2017.
- [25] S. Y. Hou, W. C. Chen, C. Hu, C. Chiu, K. C. Ting, T. S. Lin, W. H. Wei, W. C. Chiou, V. J. C. Lin, V. C. Y. Chang, C. T. Wang, C. H. Wu, and D. Yu, "Wafer-Level Integration of an Advanced Logic-Memory System Through the Second-Generation CoWoS Technology," *IEEE Transactions on Electron Devices*, vol. 64, no. 10, 2017.
- [26] C. Hu, M. Chen, W. Chiou, and D. Yu, "3D Multi-chip Integration with System on Integrated Chips (SoIC)," in *Symposium on VLSI Technology*, 2019.
- [27] I. Hubara, M. Courbariaux, D. Soudry, R. El-Yaniv, and Y. Bengio, "Binarized Neural Networks," in *Advances in Neural Information Processing Systems 29*, 2016.
- [28] D. Ingerly, K. Enamul, W. Gomes, D. Jones, K. Kolluru, A. Kandas, G.-S. Kim, H. Ma, D. Pantuso, C. Petersburg, M. Phen-givoni, A. Pillai, A. Sairam, P. Shekhar, P. Sinha, P. Stover, A. Telang, Z. Zell, and R. Criss, "Foveros: 3D Integration and the use of Face-to-Face Chip Stacking for Logic Devices," in *IEEE International Electron Devices Meeting (IEDM)*, 2019.
- [29] "14 nm Technology Announcement," 2015. [Online]. Available: <https://www.intel.com/content/dam/www/public/us/en/documents/presentation/advancing-moores-law-in-2014-presentation.pdf>
- [30] "Lakefield: Hybrid cores in 3D Package." 2019. [Online]. Available: https://www.hotchips.org/hc31/HC31_2.10_LKF_HC_2019_Final_v7.pdf
- [31] Z. Jia, B. Tillman, M. Maggioni, and D. P. Scarpazza, "Dissecting the Graphcore IPU Architecture via Microbenchmarking," in *arXiv preprint arXiv:1912.03413*, 2019.
- [32] Y. Jiao, L. Han, R. Jin, Y.-J. Su, C. Ho, L. Yin, Y. Li, L. Chen, Z. Chen, L. Liu, Z. He, Y. Yan, J. He, J. Mao, X. Zai, X. Wu, Y. Zhou, M. Gu, G. Zhu, R. Zhong, W. Lee, P. Chen, Y. Chen, W. Li, D. Xiao, Q. Yan, M. Zhuang, J. Chen, Y. Tian, Y. Lin, W. Wu, H. Li, and Z. Dou, "A 12nm Programmable Convolution-Efficient Neural-Processing-Unit Chip Achieving 825TOPS," in *International Solid-State Circuits Conference (ISSCC)*, 2020.
- [33] N. P. Jouppi, D. H. Yoon, G. Kurian, S. Li, N. Patil, J. Laudon, C. Young, and D. Patterson, "A Domain-Specific Supercomputer for Training Deep Neural Networks," *Communications of the ACM*, vol. 63, no. 7, 2020.
- [34] N. P. Jouppi, C. Young, N. Patil, D. Patterson, G. Agrawal, R. Bajwa, S. Bates, S. Bhatia, N. Boden, A. Borchers, R. Boyle, P.-I. Cantin, C. Chao, C. Clark, J. Coriell, M. Daley, M. Dau, J. Dean, B. Gelb, T. V. Ghaemmaghami, R. Gottipati, W. Gulland, R. Hagmann, C. R. Ho, D. Hogberg, J. Hu, R. Hundt, D. Hurt, J. Ibarz, A. Jaffey, A. Jaworski, A. Kaplan, H. Khaitan, D. Killebrew, A. Koch, N. Kumar, S. Lacy, J. Laudon, J. Law, D. Le, C. Leary, Z. Liu, K. Lucke, A. Lundin, G. MacKean, A. Maggiore, M. Mahony, K. Miller, R. Nagarajan, R. Narayanaswami, R. Ni, K. Nix, T. Norrie, M. Omernick, N. Penukonda, A. Phelps, J. Ross, M. Ross, A. Salek, E. Samadiani, C. Severn, G. Sizikov, M. Snellman, J. Souter, D. Steinberg, A. Swing, M. Tan, G. Thorson, B. Tian, H. Toma, E. Tuttle, V. Vasudevan, R. Walter, W. Wang, E. Wilcox, and D. H. Yoon, "In-Datacenter Performance Analysis of a Tensor Processing Unit," in *International Symposium on Computer Architecture (ISCA)*, 2017.

- [35] A. Kannan, N. Enright Jerger, and G. Loh, "Enabling Interposer-based Disintegration of Multi-core Processors," in *International Symposium on Networks-on-Chip (NOCS)*, 2015.
- [36] J. Kaplan, S. McCandlish, T. Henighan, T. B. Brown, B. Chess, R. Child, S. Gray, A. Radford, J. Wu, and D. Amodei, "Scaling Laws for Neural Language Models," in *arXiv preprint arXiv:2001.08361*, 2020.
- [37] S. Keckler, W. Dally, B. Khailany, M. Garland, and D. Glasco, "GPUs and the Future of Parallel Computing," *IEEE Micro*, vol. 31, no. 5, 2011.
- [38] M. Khairy, Z. Shen, T. M. Aamodt, and T. G. Rogers, "Accel-sim: An extensible simulation framework for validated gpu modeling," in *International Symposium on Computer Architecture (ISCA)*, 2020.
- [39] B. Klenk, N. Jiang, G. Thorson, and L. Dennison, "An In-Network Architecture for Accelerating Shared-Memory Multiprocessor Collectives," in *International Symposium on Computer Architecture (ISCA)*, 2020.
- [40] F. Li, B. Zhang, and B. Liu, "Ternary Weight Networks," in *arXiv:1605.04711*, 2016.
- [41] Y. Li, I.-J. Liu, Y. Yuan, D. Chen, A. Schwing, and J. Huang, "Accelerating distributed reinforcement learning with in-switch computing," in *International Symposium on Computer Architecture (ISCA)*, 2019.
- [42] S. Lie, "Wafer Scale Deep Learning," in *HotChips-31*, 2019.
- [43] M.-S. Lin, T.-C. Huang, C.-C. Tsai, K.-H. Tam, C.-H. Hsieh, T. Chen, W.-H. Huang, J. Hu, Y.-C. Chen, S. Goel, C.-M. Fu, S. Rusu, C.-C. Li, S.-Y. Yang, M. Wong, S.-C. Yang, and F. Lee, "A 7nm 4GHz Armcore-based CoWoS Chiplet Design for High Performance Computing," in *Symposium on VLSI Circuits*, 2019.
- [44] "Laghos." [Online]. Available: <https://computing.llnl.gov/projects/codesign/laghos>
- [45] "The CORAL Benchmarks," 2014. [Online]. Available: <https://asc.llnl.gov/CORAL-benchmarks/>
- [46] "The CORAL2 Benchmarks," 2017. [Online]. Available: <https://asc.llnl.gov/coral-2-benchmarks>
- [47] G. H. Loh, N. E. Jerger, A. Kannan, and Y. Eckert, "Interconnect-Memory Challenges for Multi-Chip, Silicon Interposer Systems," in *International Symposium on Memory Systems*, 2015.
- [48] P. Mattson, C. Cheng, G. Diamos, C. Coleman, P. Micikevicius, D. Patterson, H. Tang, G.-Y. Wei, P. Bailis, V. Bittorf, D. Brooks, D. Chen, D. Dutta, U. Gupta, K. Hazelwood, A. Hock, X. Huang, D. Kang, D. Kanter, N. Kumar, J. Liao, D. Narayanan, T. Oguntebi, G. Pekhimenko, L. Pentecost, V. Janapa Reddi, T. Robie, T. St John, C.-J. Wu, L. Xu, C. Young, and M. Zaharia, "MLPerf Training Benchmark," in *Machine Learning and Systems (MLSys)*, 2020.
- [49] P. Micikevicius, S. Narang, J. Alben, G. Diamos, E. Elsen, D. Garcia, B. Ginsburg, M. Houston, O. Kuchaiev, G. Venkatesh, and H. Wu, "Mixed Precision Training," in *International Conference on Learning Representations (ICLR)*, 2018.
- [50] U. Milic, O. Villa, E. Bolotin, A. Arunkumar, E. Ebrahimi, A. Jaleel, A. Ramirez, and D. Nellans, "Beyond the Socket: NUMA-aware GPUs," in *International Symposium on Microarchitecture (MICRO)*, 2017.
- [51] "MLPerf Inference Results v0.5," 2019. [Online]. Available: <https://mlperf.org/inference-results/>
- [52] "MLPerf Training Results v0.6," 2019. [Online]. Available: <https://mlperf.org/training-results-0-6/>
- [53] G. E. Moore, "Cramming More Components onto Integrated Circuits," *Electronics*, 1965.
- [54] S. Naffziger, K. Lepak, M. Paraschou, and M. Subramony, "AMD Chiplet Architecture for High-Performance Server and Desktop Products," in *International Solid-State Circuits Conference (ISSCC)*, 2020.
- [55] "FUN3D." [Online]. Available: <https://fun3d.larc.nasa.gov/>
- [56] "NVIDIA Kepler GK110 Architecture," 2012. [Online]. Available: <https://www.nvidia.com/content/PDF/kepler/NVIDIA-Kepler-GK110-Architecture-Whitepaper.pdf>
- [57] "NVIDIA NVLink," 2016. [Online]. Available: <https://www.nvidia.com/en-us/data-center/nvlink/>
- [58] "NVIDIA Tesla P100 Architecture," 2016. [Online]. Available: <https://images.nvidia.com/content/pdf/tesla/whitepaper/pascal-architecture-whitepaper.pdf>
- [59] "NVIDIA Tesla V100 Architecture," 2017. [Online]. Available: <http://images.nvidia.com/content/volta-architecture/pdf/volta-architecture-whitepaper.pdf>
- [60] "NVIDIA Turing GPU Architecture," 2019. [Online]. Available: <https://www.nvidia.com/content/dam/en-zz/Solutions/design-visualization/technologies/turing-architecture/NVIDIA-Turing-Architecture-Whitepaper.pdf>
- [61] "NVIDIA A100 Tensor Core GPU Architecture," 2020. [Online]. Available: <https://www.nvidia.com/content/dam/en-zz/Solutions/Data-Center/nvidia-ampere-architecture-whitepaper.pdf>
- [62] "Open Specification for a Liquid Cooled Server Rack - Progress Update," 2018. [Online]. Available: <https://datacenters.lbl.gov/sites/default/files/OpenSpecification.pdf>
- [63] S. Pal, E. Ebrahimi, A. Zulfiqar, Y. Fu, V. Zhang, S. Migacz, D. Nellans, and P. Gupta, "Optimizing Multi-GPU Parallelization Strategies for Deep Learning Training," *IEEE Micro*, vol. 39, no. 5, 2019.
- [64] V. Pano, R. Kuttappa, and B. Taskin, "3D NoCs with Active Interposer for Multi-Die Systems," in *International Symposium on Networks-on-Chip (NOCS)*, 2019.
- [65] V. J. Reddi, C. Cheng, D. Kanter, P. Mattson, G. Schmuelling, C. Wu, B. Anderson, M. Breughe, M. Charlebois, W. Chou, R. Chukka, C. Coleman, S. Davis, P. Deng, G. Diamos, J. Duke, D. Fick, J. S. Gardner, I. Hubara, S. Idgunji, T. B. Jablin, J. Jiao, T. S. John, P. Kanwar, D. Lee, J. Liao, A. Lokhmotov, F. Massa, P. Meng, P. Micikevicius, C. Osborne, G. Pekhimenko, A. T. R. Rajan, D. Sequeira, A. Sirasao, F. Sun, H. Tang, M. Thomson, F. Wei, E. Wu, L. Xu, K. Yamada, B. Yu, G. Yuan, A. Zhong, P. Zhang, and Y. Zhou, "MLPerf Inference Benchmark," in *International Symposium on Computer Architecture (ISCA)*, 2020.
- [66] X. Ren, D. Lustig, E. Bolotin, A. Jaleel, O. Villa, and D. Nellans, "HMG: Extending Cache Coherence Protocols Across Modern Hierarchical Multi-GPU Systems," in *International Symposium on High-Performance Computer Architecture (HPCA)*, 2020.
- [67] O. Ronneberger, P. Fischer, and T. Brox, "U-Net: Convolutional Networks for Biomedical Image Segmentation," in *arXiv:1505.04597*, 2015.
- [68] A. Sallab, M. Abdou, E. Perot, and S. Yogamani, "Deep Reinforcement Learning framework for Autonomous Driving," *Electronic Imaging*, 2017.
- [69] Y. S. Shao, J. Clemons, R. Venkatesan, B. Zimmer, M. Fojtik, N. Jiang, B. Keller, A. Klinefelter, N. Pinckney, P. Raina, S. G. Tell, Y. Zhang, W. J. Dally, J. Emer, C. T. Gray, B. Khailany, and S. W. Keckler, "Simba: Scaling Deep-Learning Inference with Multi-Chip-Module-Based Architecture," in *International Symposium on Microarchitecture (MICRO)*, 2019.
- [70] Y. Sun, Y. Chen, X. Wang, and X. Tang, "Deep Learning Face Representation by Joint Identification-Verification," in *International Conference on Neural Information Processing Systems*, 2014.
- [71] W. J. Turner, J. W. Poulton, J. M. Wilson, X. Chen, S. G. Tell, M. Fojtik, T. H. Greer, B. Zimmer, S. Song, N. Nedovic, S. S. Kudva, S. R. Sudhakaran, R. Bashirullah, W. Zhao, W. J. Dally, and C. T. Gray, "Ground-Referenced Signaling for Intra-Chip and Short-Reach Chip-to-Chip Interconnects," in *IEEE Custom Integrated Circuits Conference (CICC)*, 2018.
- [72] V. Vashishtha, M. Vangala, P. Sharma, and L. T. Clark, "Robust 7-nm SRAM Design on a Predictive PDK," in *International Symposium on Circuits and Systems (ISCAS)*, 2017.
- [73] O. Villa, D. Lustig, Z. Yan, E. Bolotin, Y. Fu, N. Chatterjee, N. Jiang, and D. Nellans, "Need for speed: Experiences building a trustworthy system-level gpu simulator," in *International Symposium on High-Performance Computer Architecture (HPCA)*, 2021.
- [74] P. Vivet, E. Guthmuller, Y. Thonnart, G. Pillonnet, G. Moritz, I. Miro-Panadès, C. Fuguet, J. Durupt, C. Bernard, D. Varreau, J. Pontes, S. Thuries, D. Coriat, M. Harrand, D. Dutoit, D. Lattard, L. Arnaud, J. Charbonnier, P. Coudrain, A. Garnier, F. Berger, A. Gueugnot, A. Greiner, Q. Meunier, A. Farcy, A. Arriordaz, S. Cheramy, and F. Clermidy, "A 220 GOPS 96 Core Processor with 6 Chiplets 3D-Stacked on an Active Interposer Offering 0.6ns/mm Latency, 3Tb/s/mm2 Inter-Chiplet Interconnects and 156mW/mm2 at 82%-Peak-Efficiency DC DC Converters," in *International Solid-State Circuits Conference (ISSCC)*, 2020.
- [75] V. Young, A. Jaleel, E. Bolotin, E. Ebrahimi, D. Nellans, and O. Villa, "Combining HW/SW Mechanisms to Improve NUMA Performance of Multi-GPU Systems," in *International Symposium on Microarchitecture (MICRO)*, 2018.